Thorax Design and Wing Control for a Micromechanical Flying Insect*

J. Yan, S. Avadhanula, M. Sitti, R.J. Wood and R.S. Fearing

Dept. of Electrical Engineering & Computer Sciences
University of California, Berkeley
Berkeley, CA 94720
{joeyan, srinath, sitti, rjwood, ronf}@eecs.berkeley.edu

Abstract

Inspired by biological insect flight, the UC Berkeley Micromechanical Flying Insect project aims to develop a robot capable of autonomous flight through the use of a pair of flapping wings. A 2 degree-of-freedom resonant thorax structure has been designed and fabricated. Miniature piezoelectric PZN-PT unimorph actuators have been fabricated and can provide sufficient power for the MFI. Instrumentation with strain gauges will allow force sensing for closed-loop wing control.

1 Introduction

The micromechanical flying insect (MFI) project entails the development of a centimeter-scale robot capable of flying using flapping wings. Commercial and military applications for micro aerial vehicles such as this include operations in hazardous environments (*e.g.,* search-and-rescue within collapsed buildings, nuclear plant exploration during a radiation leak, *etc.*) and defense-related missions (*e.g.,* reconnaissance and surveillance).

Although several groups have worked on MAVs based on fixed or rotary wings (*e.g.* [10]), flapping flight provides superior maneuverability which would be beneficial in obstacle avoidance and necessary for navigation in small spaces, as demonstrated by biological flying insects. It has long been known that insect flight cannot be explained by steady state aerodynamics and only in recent years has there been elucidation of the unsteady aerodynamic mechanisms which account for the large lift forces generated. Francis and Cohen appear to have been the first to study impulsive wing translational motions which give rise to the phenomenon known as *delayed stall* [6]; this effect has recently been quantified using a scaled model of a hawkmoth by Ellington *et al* [4]. Dickinson *et al* observed that this phenomenon was inadequate in accounting for the total lift and, using a dynamically-scaled model of a fruitfly, established two additional important lift mechanisms: *rotational circulation* and *wake capture* [3]. The success of flapping MAVs depends on exploitation of all three mechanisms.

Shimoyama pioneered work in micro-robotic flight ([16], [7]) while milli-robotic flapping flight has been pursued by several other groups ([2], [13]). Prior work on the MFI has been documented in several areas by Fearing *et al* [5], Yan *et al* [21], Sitti *et al* [17], and Schenato *et al* [14].

*This research supported by ONR MURI N00014-98-1-0671 and DARPA

2 Thorax Design

Figure 1 illustrates the proposed components of the MFI along with a photo of a mock-up, fabricated to scale (but without actuation).

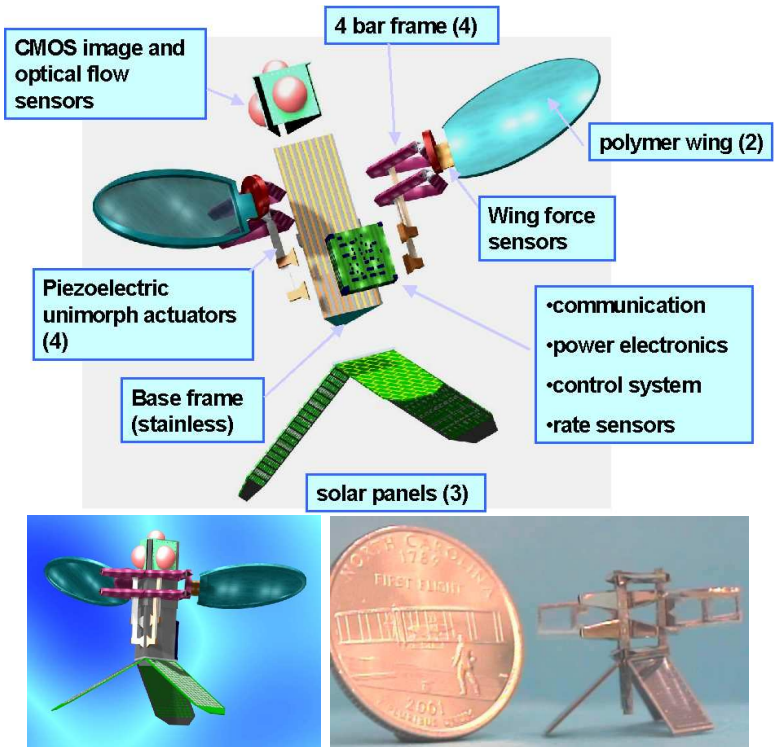

Figure 1: (a) Pre-assembled view showing modular components; (b) Conceptual rendition of MFI; and (c) Structural mock-up at final scale.

Insect flight at the centimeter scale requires both large stroke amplitude and wing rotation [3]. Drosophila uses a wing stroke of 160° combined with wing rotation of over 90°. The design target for the biologically-inspired MFI is the blowfly Calliphora. The MFI specifications are summarized in Table 1 and match the values of the blowfly for total mass, wing length, wing beat frequency, and actuation power.

Parameter	Specification
Resonance frequency	150 Hz
Wingspan	25 mm
Stroke angle range	140°
Rotation angle range	90°
Wing power available	8 mW
Thorax mass	67 mg
Wing mass (per wing)	0.5 mg
Total mass budget	100 mg

Table 1: MFI specifications

The thorax of a biological insect uses a complicated arrangement of linkages and cams [11] which is not fully understood and is too difficult to fabricate. For each wing, the

MFI thorax design, illustrated in Figure 2, uses a pair of 4-bar frames to control two links of a spherical 5-bar mechanism, permitting the necessary 2 degrees of freedom (DOF).

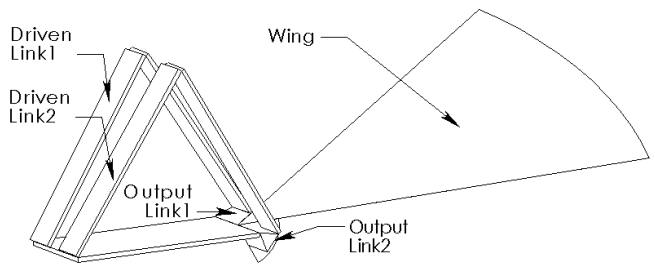

Figure 2: Assembly of the planar 4-bar pair with a spherical 5-bar permits wing flapping and rotation.

2.1 Thorax Kinematics

Figure 3(a) shows a 1 DOF planar 4-bar mechanism with link 1 fixed. For a given driven link angle θ_2, the output link angle θ_4 can take on two possible values corresponding to two valid 4-bar configurations. Knowing the initial configuration, the forward kinematics can uniquely be determined if singularities are avoided.

For link lengths $l_1 = l_2 = l_3 = 5mm$ and $l_4 = 1mm$, the 4-bar input/output characteristics are shown in Figure 3(b). The driven link moves beween 47° and 74° (a range of 27°) to provide output motion between $-66°$ and 117° (a range of 173°). Thus, the angular motion magnification is 6.4 when operating over the entire range although the value is much closer to 5 near the nominal operating point. This magnification allows piezoelectric unimorph actuators, described in Section 2.3, to be used even though they have very small output displacements.

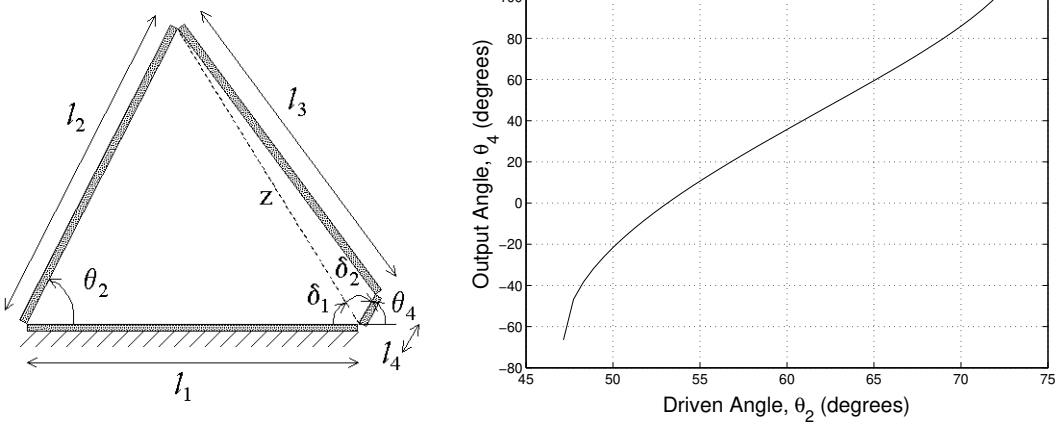

Figure 3: (a) Planar 4-bar kinematics and (b) Input/Output characteristics with link lengths $l_1 = l_2 = l_3 = 5mm$ and $l_4 = 1mm$.

The spherical 5-bar differential is shown in Figure 4(a). The planar links **AOB** and **EOD** are rigidly attached to the output links of the 4-bars and are driven about the z-axis by angles $\theta_{\mathbf{AOB}}$ and $\theta_{\mathbf{EOD}}$ as shown. By fixing one of these links, the mechanism is

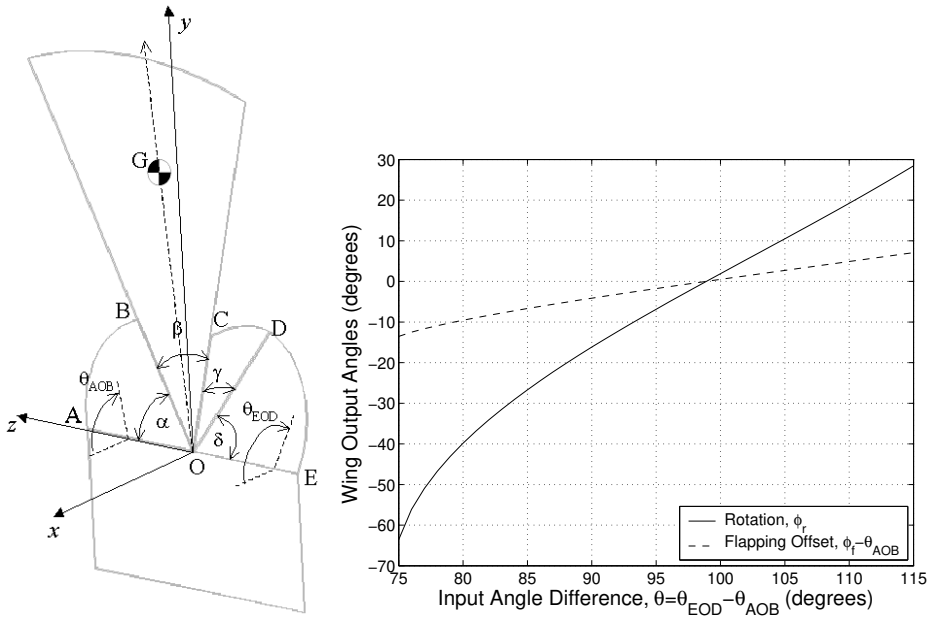

Figure 4: (a) Spherical 5-bar kinematics and (b) Input/Output characteristics with vertex angles $\alpha = \gamma = \delta = 75°$ and $\beta = 30°$.

reduced to a spherical 4-bar for which the kinematic analysis can be found in a standard text on linkages and mechanisms such as [9] by McCarthy.

The wing rotation angle ϕ_r is naturally defined as the angle made between planes **AOB** and **BOC** and depends only on the link angle difference $\theta = \theta_{\mathbf{EOD}} - \theta_{\mathbf{AOB}}$. As with the 4-bar, there are two solutions for this wing rotation but it is uniquely determined for an initial configuration when singularities are avoided. Figure 4(b) shows ϕ_r as a function of θ for a wing differential with one set of physical parameters for which wing rotation over 90° can be achieved by changing θ over a range of 40°.

The flapping angle ϕ_f is not so naturally defined and several candidates come to mind. ϕ_f may reasonably be based on motion of the wing leading edge, the center of area, the wing angular bisector, the intersection between the wing and the stroke plane, or simply the average of the driven link angles (*i.e.*, $\phi_f = (\theta_{\mathbf{AOB}} + \theta_{\mathbf{EOD}})/2$). For this paper, the flapping angle is based on the motion of the wing center of area **G**. If a flat plate with one edge hinged to the z-axis is rotated so that it coincides with **G**, then ϕ_f will be the angle made between the plate and the $+x$-axis. This can be found by projecting **G** onto the x-y plane and finding the angle that this projected vector makes with the x-axis. ϕ_f depends on θ but is offset by $\theta_{\mathbf{AOB}}$ (only $\phi_f - \theta_{\mathbf{AOB}}$ needs to be plotted, as is done in Figure 4(b)). For limited input angle ranges for $\theta_{\mathbf{AOB}}$ and $\theta_{\mathbf{EOD}}$, the ranges for ϕ_r and ϕ_f are coupled and one may be increased at the expense of the other. It should also be observed that $\phi_r = 0°$ near $\theta = 98°$ and the structure would have this nominal difference by construction.

2.2 Thorax and Wing Construction

Pin joints are difficult to place in the small structures of MFI and they suffer problems with friction, wear, reinforcement, and alignment. Instead, flexures are employed to allow rotational motion between links. Polyester flexures $6.25\mu m$ thick and $125\mu m$ long are suitable as they have been tested over 10^6 cycles without failure and they have very low

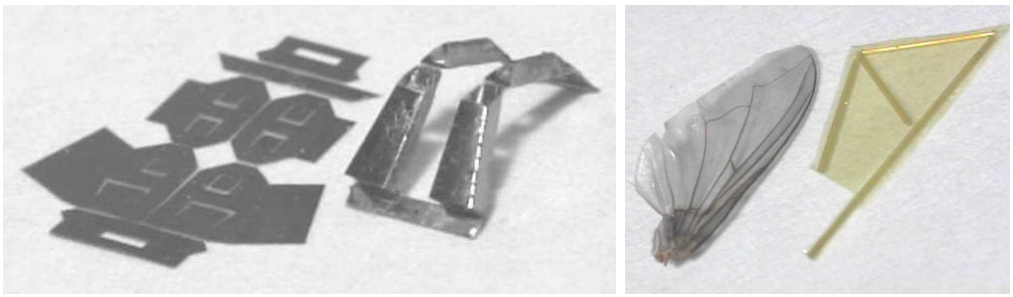

Figure 5: (a) Laser-cut pattern for thorax dual 4-bar flexural frame before and after folding. (b) $0.5mg$ polyimide wing, shown with Calliphora wing for comparison.

stiffness.

MFI structures need to have a high strength-to-weight ratio and this is achieved using hollow beams which can be several orders of magnitude stiffer than a solid beam of the same mass [22]. The hollow structures are folded up from $12.5\mu m$ thick stainless steel shim. Figure 5(a) illustrates a laser-cut template which can be folded into the dual 4-bar structure beside it. By keeping the pair of 4-bars on the same template, alignment problems are reduced. The polyester flexures employed at each joint are glued to the flat template before folding.

Currently, the structures are folded manually using fixtures and bonded using cyanoacrylate adhesive. Automated folding of microstructures is quite feasible, particularly using simple fixtures and a motion planning approach such as that described by Lu and Akella in [8]. Tools for microassembly are described by Shimada *et al* in [15] and by Thompson and Fearing in [19].

Lightweight wings are fabricated with a polyimide spincoating step resulting in a final thickness of $7\mu m$. The wings are reinforced with $200\mu m$ diameter polyimide tubes to provide rigidity. Each wing weighs $0.5mg$ and has an inertia moment of $20mg \cdot mm^2$. Figure 5(b) shows the resulting wing beside the wing of a blowfly for comparison.

2.3 Actuation

The basic MFI actuator is the piezoelectric unimorph, shown in Figure 6 and described by Sitti *et al* [17]. The beam theory for unimorph actuators is well established [18] and they have been used previously by Cox *et al* for flapping mechanisms [2]. The MFI unimorph consists of a single-crystal PZN-PT piezoelectric layer bonded to a steel elastic layer. Application of an electric field across the piezoelectric layer gives rise to longitudinal and transverse strains which lead to bending.

Unimorph actuator design parameters such as the dimensions, output torque, transmission ratio, quality factor, weight, *etc.* can be selected for optimal performance. Calculations indicate that each wing of the MFI can be driven by a pair of unimorphs, each having dimensions $5mm \times 1.1mm \times (90\mu m$ PZN-PT $+35.6\mu m$ steel) and weighing $5mg$ (*i.e.*, the total MFI actuator mass would be $20mg$, or 20% of the overall mass).

2.4 Force Sensing

Insects such as Calliphora use a sophisticated means to measure forces and torques for complicated guidance systems [12], [1]. MFI force measurements will serve the dual purpose of stroke force characterization and sensor feedback in the real-time wing control

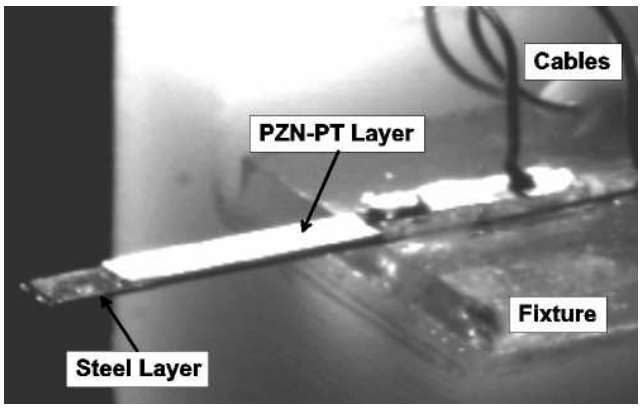

Figure 6: Photo of $5 \times 1 \times 0.22$ mm^3 PZN-PT unimorph.

system. The sensors need to have high sensitivity (the expected force range is on the order of a few mN) and high bandwidth (at least an order of magnitude higher than the wingbeat frequency of $150Hz$).

MFI wing force measurements have been taken using semiconductor strain gauges mounted directly on the wing spars as shown in Figure 7 and described by Wood and Fearing [20].

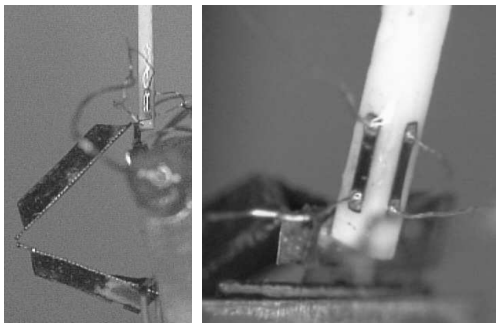

Figure 7: Photos of $1mm$ strain gauge mounted on 1.3X spar (a) attached to a four-bar and (b) close-up of wiring.

During a wing stroke, a force distribution develops along the wing spar. For a rigid body, this force distribution can be reduced to a single force vector acting at the center of force of the distribution. The signals measured include both aerodynamic and inertial forces, the latter accounting for up to 90% of the measurement.

Since the wing must go through large stroke and rotation angles, the wiring to the gauges presents problems both in terms of fatigue and with added parallel stiffness. To overcome this problem, the strain gauges may be placed at either the 4-bar base or the unimorph actuator and then, utilizing the differential mapping, wing forces may be estimated. Wiring of the gauges at the final scale is also extremely difficult. To alleviate this, a wing fabricated using MEMS technology is being pursued, with built-in strain gauges and amplification circuitry.

3 Wing Control

An overview of the proposed MFI hierarchical control architecture has been presented by Schenato *et al* [14]. In this scheme, the mission planner is at the highest level, followed

by the trajectory planner, the flight mode controller and finally, the wing kinematics controller. This section discusses issues related only to the wing controller which tracks desired force or position trajectories and is vital for all other levels to work.

A block diagram of the wing control system is shown in Figure 8. The control input $u(t)$ depends on the desired reference trajectory $r(t)$ and the estimated wing states $\hat{x}(t)$. $r(t)$, generated on a half-stroke-by-half-stroke basis (as explained in Section 3.2), is passed down from the flight mode controller and may be a desired force or position signal.

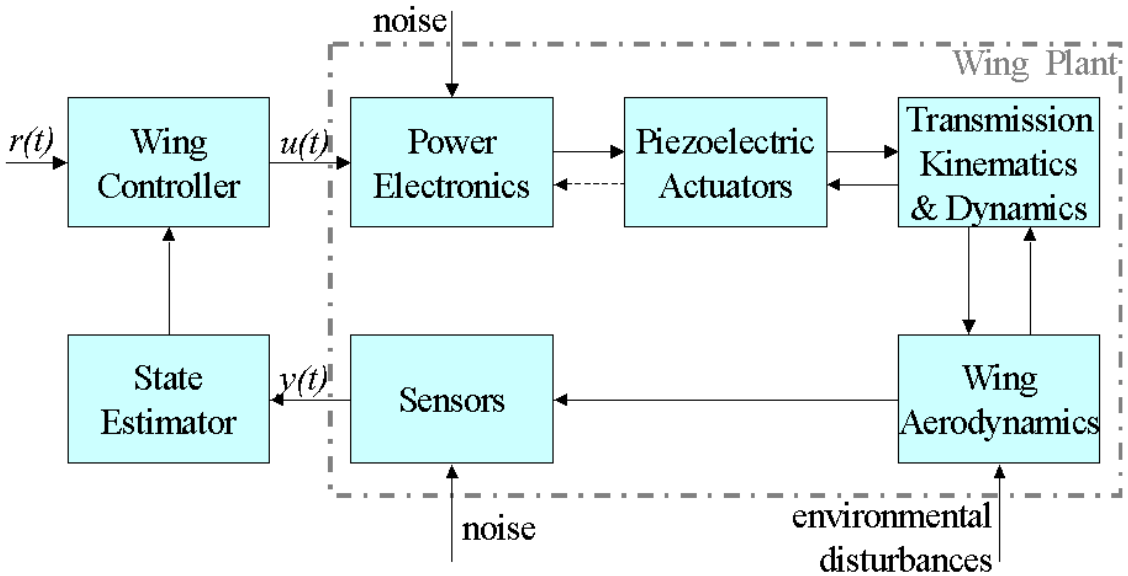

Figure 8: Block diagram of wing control model

3.1 Structural Dynamics

A dynamic model for the wing plant can be derived using Lagrangian mechanics. For the MFI, the equations of motion would include many nonlinearities but insight for the control can be derived even from a simplified dynamic model such as the one shown in Figure 9 comprised only of linear elements.

For a large transmission ratio T from actuator input angle to spar output angle, 4-bar inertia and damping terms become negligible. This simplified model results in a fourth order system with two inputs and two outputs. This system has two resonant frequencies which have in-phase (flapping) and out-of-phase (rotational) natural motion modes given by:

$$\begin{aligned} \omega_f^2 &= \frac{2\kappa_1}{T^2 J_f} \\ \omega_r^2 &= \frac{\kappa_1 + 2\kappa_d}{2\lambda^2 T^2 J_r} \end{aligned} \tag{1}$$

where λ is the gain from spar angle difference to wing rotation angle (from θ to ϕ_r, using the notation of Section 2.1). The parameters should be chosen so that these frequencies are closely matched so that simultaneous flapping and rotation can be achieved at resonance as illustrated in the sample wing trajectory of Figure 10. If there is a large difference between these frequencies, undesirable vibrational modes may be excited or insufficient motion may be generated for a desired mode.

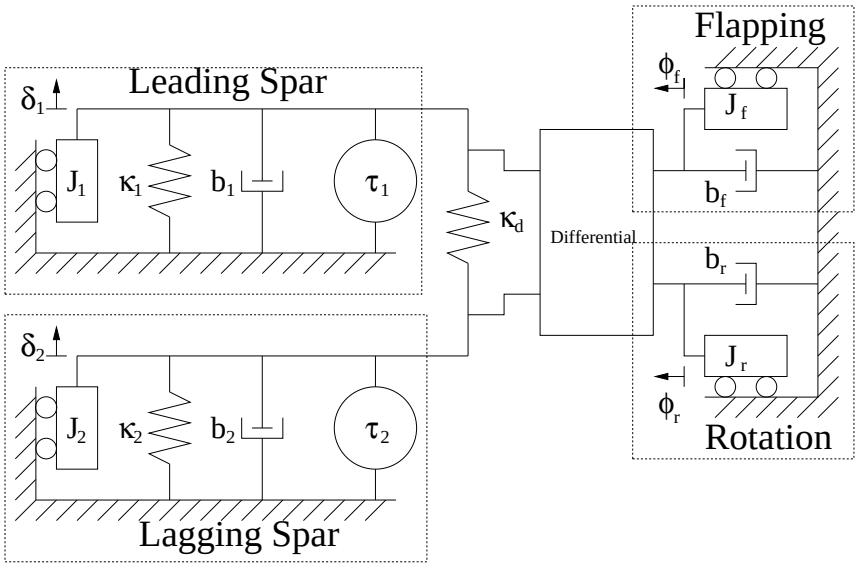

Figure 9: Model of 2 DOF Dynamics (composed of rotational elements but illustrated with the more familiar translational analogs)

3.2 Other control issues

The thorax will be driven near resonance, a mode which is typically purposely suppressed in most control applications. As a result, the phase lag between the input actuation signal and the motion is 90^o, effectively introducing a "time delay" into the control. Thus, there are no ways to control the position of the wing except on a half-stroke-by-half-stroke basis; there is evidence to suggest this is true even for biological flying insects.

A switching controller, which sets the piezoelectric unimorph voltage at $0V$ or $+V_{max}$, will be used but this adds complexity to the problem. Although continuous-time equations of motion can be derived, the wing controller becomes a hybrid system because of the discrete output levels. Nonlinear terms in the dynamic equations are introduced by the thorax kinematics, the PZN-PT saturation and the aerodynamic drag. In addition, time-varying terms arise from the PZN-PT hysteresis and rom the unsteady aerodynamic forces.

Robustness will be an important concern and stochastic models of the noise and disturbances which may be encountered (*e.g.,* measurement noise, wind gusts, *etc.*) need to be developed before tackling this problem.

4 Conclusion

At this stage in the MFI design, a good understanding of the necessary wing kinematics, forces, velocities and power has been developed from measurements on Robofly and real insects. Kinematic structures at the desired size scale have been fabricated using folded stainless steel to give adequate wing motion when driven by piezoelectric unimorph actuators. Instrumentation of the MFI with strain gauges and other sensors will permit the wing forces to be quantified. Closed-loop wing controllers are being developed to react to wing forces and modify wing stroke patterns as needed to achieve stable flight.

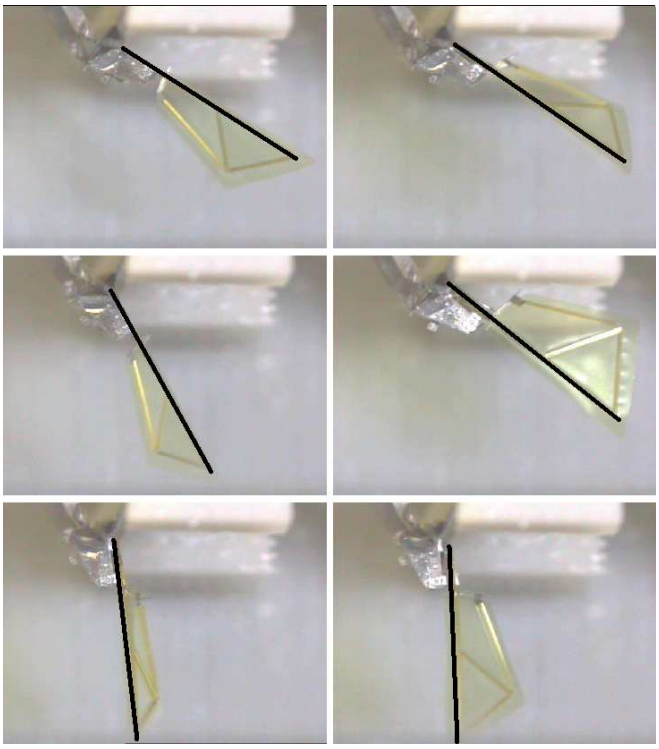

Figure 10: Clockwise sequence of images for a wing prototype driven at $100Hz$ with a rotation range of over 90° and flapping range of 80°. The dark line indicates the leading edge of the wing. The first 3 images in the sequence (starting from the top left) illustrate wing rotation at the end of a stroke.

References

[1] J.H. Cocatre-Zilgien and F. Delcomyn. Modeling stress and strain in an insect leg for simulation of campaniform sensilla responses to external forces. *Biological Cybernetics*, 81(2):149–60, Aug 1999.

[2] A. Cox, E. Garcia, and M. Goldfarb. Actuator development for a flapping microrobotic MAV. In *SPIE Microrobotics Symp*, pages 102–8, Boston, MA, Nov 1998.

[3] M.H. Dickinson, F-O. Lehmann, and S.P. Sane. Wing rotation and the aerodynamic basis of insect flight. *Science*, 284:1954–60, June 1999.

[4] C.P. Ellington, C. van den Berg, A.P. Willmot, and A.L.R. Thomas. Leading edge vortices in insect flight. *Nature*, 384:626–30, December 1996.

[5] R.S. Fearing, K.H. Chiang, M.H. Dickinson, D.L. Pick, M. Sitti, and J. Yan. Wing transmission for a micromechanical flying insect. In *Proc of IEEE Intl Conf on Robotics and Automation*, pages 1509–16, San Francisco, CA, April 2000.

[6] R.H. Francis and J. Cohen. The flow near a wing which starts suddenly from rest and then stalls. *Rep Memo Aeronaut Res Comm*, 1561, 1933.

[7] Y. Kubo, I. Shimoyama, T. Kaneda, and H. Miura. Study on wings of flying microrobots. In *Proc of IEEE Intl Conf on Robotics and Automation*, pages 834–9, San Diego, CA, May 1994.

[8] L. Lu and S. Akella. Folding cartons with fixtures: A motion planning approach. In *Proc of IEEE Intl Conf on Robotics and Automation*, pages 1570–6, Detroit, MI, May 1999.

[9] J.M. McCarthy. *Geometric Design of Linkages*. Springer-Verlag, 2000.

[10] B. Motazed, D. Vos, and M. Drela. Aerodynamics and flight control design for hovering MAVs. In *Proc of Amer Control Conf*, Philadelphia, PA, June 1998.

[11] W. Nachtigall, A. Wisser, and D. Eisinger. Flight of the honey bee. VIII. functional elements and mechanics of the 'flight motor' and the wing joint - one of the most complicated gear-mechanisms in the animal kingdom. *J. Comp. Physiology B*, 168:323–44, 1998.

[12] G. Nalbach. The halteres of the blowfly calliphora. *Journal of Comparitive Physiology*, (173):293–300, 1993.

[13] T.N. Pornsin-Sirirak, S.W. Lee, H. Nassef, J. Grasmeyer, Y.C. Tai, C.M. Ho, and M. Keennon. MEMS wing technology for a battery-powered ornithopter. In *Proc. of IEEE 13th Annual Intl Conf on MEMS*, pages 799–804, Piscataway, NJ, Jan 2000.

[14] L. Schenato, X. Deng, W.C. Wu, and S. Sastry. Flight control system for a micromechanical flying insect: Architecture and implementation. In *Proc of IEEE Intl Conf on Robotics and Automation*, pages 1641–6, Seoul, Korea, May 21-36 2001.

[15] E. Shimada, J.A. Thompson, J. Yan, R.J. Wood, and R.S. Fearing. Prototyping millirobots using dextrous microassembly and folding. In *Symp on Microrobotics ASME Intl Mech Eng Cong and Expo*, Orlando, FL, Nov 5-10 2000.

[16] I. Shimoyama, H. Miura, K. Suzuki, and Y. Ezura. Insect-like microrobots with external skeletons. *IEEE Control Systems Magazine*, 13:37–41, February 1993.

[17] M. Sitti, D. Campolo, J. Yan, R.S. Fearing, T. Su, D. Taylor, and T.D. Sands. Development of PZT and PZN-PT based unimorph actuators for micromechanical flapping mechanisms. In *Proc of IEEE Intl Conf on Robotics and Automation*, pages 3839–46, Seoul, Korea, May 21-36 2001.

[18] J. Smits and W. Choi. The constituent equations of piezoelectric heterogenous bimorphs. *IEEE Tran. on Ultrasonics, Ferroelectrics, and Freq Control*, 38:256–70, May 1991.

[19] J.A. Thompson and R.S. Fearing. Automating microassembly with ortho-tweezers and force sensing. In *to appear, IROS 2001*, Maui, HI, Oct 29-Nov 3 2001.

[20] R.J. Wood and R.S. Fearing. Flight force measurements for a micromechanical flying insect. In *to appear, IROS 2001*, Maui, HI, Oct 29-Nov 3 2001.

[21] J. Yan, R.J. Wood, S. Avadhanula, M. Sitti, and R.S. Fearing. Towards flapping wing control for a micromechanical flying insect. In *Proc of IEEE Intl Conf on Robotics and Automation*, pages 3901–8, Seoul, Korea, May 21-36 2001.

[22] R. Yeh, E.J. Kruglick, M. Klitzke, and K.S.J. Pister. Towards an articulated silicon microrobot. In *Winter Annual Meeting, ASME*, Dec 1994.